

Coupled Spin-Light dynamics in Cavity Optomagnonics

Silvia Viola Kusminskiy,¹ Hong X. Tang,² and Florian Marquardt^{1,3}

¹*Institute for Theoretical Physics, University Erlangen-Nürnberg, Staudtstraße 7, 91058 Erlangen, Germany*

²*Department of Electrical Engineering, Yale University, New Haven, Connecticut 06511, USA*

³*Max Planck Institute for the Science of Light, Günther-Scharowsky-Straße 1, 91058 Erlangen, Germany*

Experiments during the past two years have shown strong resonant photon-magnon coupling in microwave cavities, while coupling in the optical regime was demonstrated very recently for the first time. Unlike with microwaves, the coupling in optical cavities is parametric, akin to optomechanical systems. This line of research promises to evolve into a new field of optomagnonics, aimed at the coherent manipulation of elementary magnetic excitations by optical means. In this work we derive the microscopic optomagnonic Hamiltonian. In the linear regime the system reduces to the well-known optomechanical case, with remarkably large coupling. Going beyond that, we study the optically induced nonlinear classical dynamics of a macrospin. In the fast cavity regime we obtain an effective equation of motion for the spin and show that the light field induces a dissipative term reminiscent of Gilbert damping. The induced dissipation coefficient however can change sign on the Bloch sphere, giving rise to self-sustained oscillations. When the full dynamics of the system is considered, the system can enter a chaotic regime by successive period doubling of the oscillations.

Introduction.— The ability to manipulate magnetism has played historically an important role in the development of information technologies, using the magnetization of materials to encode information. Today’s research focuses on controlling individual spins and spin currents, as well as elementary excitations of magnetically ordered systems –denominated magnons or spin waves [1]. In particular the control of magnons is highly desirable, since their frequency is broadly tunable (ranging from MHz to THz) [2] while they can have very long lifetimes, especially for insulating materials like the ferrimagnet yttrium iron garnet (YIG) [3].

Whereas the good magnetic properties of YIG have been known since the 60s, it is only recently that coupling and controlling spin waves with electromagnetic radiation has started to be explored. Pump-probe experiments have shown ultrafast magnetization switching with light [4–6], and strong photon-magnon coupling has been demonstrated in microwave cavity experiments [7–15] –including the photon-mediated coupling between a superconducting qubit and a magnon mode [16]. Going beyond microwaves, this points to the tantalizing possibility of realizing *optomagnonics*: the coupled dynamics of magnons and photons in the optical regime, which can lead to coherent manipulation of magnons with light. The mechanism for the coupling between magnons and photons in the optical regime differs from that of the microwave regime, where resonant matching of frequencies allows for a linear coupling [17]. In the optical case, the coupling is due to the Faraday effect, where the angle of polarization of the light changes as it propagates through a magnetic material. Very recent first experiments in this regime show that this is a promising route, by demonstrating coupling between optical modes and magnons, and advances in this field are expected to develop rapidly [18–21].

In this Letter we derive and analyze the basic opto-

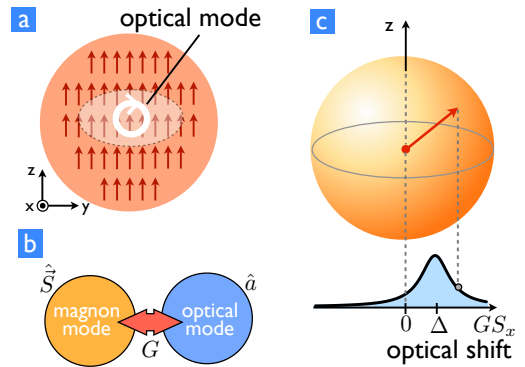


Figure 1. (Color online) Schematic configuration of the model considered. (a) Optomagnonic cavity with homogeneous magnetization along the z -axis and a localized optical mode with circular polarization in the y - z -plane. (b) The homogeneous magnon mode couples to the optical mode with strength G . (c) Representation of the magnon mode as a macroscopic spin on the Bloch sphere, whose dynamics is controlled by the coupling to the driven optical mode.

magnonic Hamiltonian that allows for the study of cavity optomagnonics. The magneto-optical coupling in this case is parametric, reminiscent of optomechanical models. This gives rise to rich non-linear dynamics even for the simple model studied here, which consists of one optical mode coupled to a homogeneous Kittel magnon mode [22]. We study the classical dynamics of the spin and find magnetization switching, self-sustained oscillations, and chaos for experimentally accessible parameters. At small magnon numbers, the ideas of optomechanics [23] carry over directly, but we will focus on the regime beyond that.

Model.— Further below, we derive the optomagnonic Hamiltonian which forms the basis of our work:

$$H = -\hbar\Delta\hat{a}^\dagger\hat{a} - \hbar\Omega\hat{S}_z + \hbar G\hat{S}_x\hat{a}^\dagger\hat{a}, \quad (1)$$

where \hat{a}^\dagger (\hat{a}) is the creation (annihilation) operator for a cavity mode photon. We work in a frame rotating at the laser frequency ω_{las} , and $\Delta = \omega_{las} - \omega_{cav}$ is the detuning vs. the optical cavity frequency ω_{cav} . Eq. (1) assumes a magnetically ordered system with (dimensionless) macrospin $\mathbf{S} = (S_x, S_y, S_z)$ with magnetization axis along $\hat{\mathbf{z}}$, and a precession frequency Ω which can be controlled by an external magnetic field [24]. The coupling between the optical field and the spin is given by the last term in Eq. (1), where we assumed (see below) that light couples only to the x -component of the spin as shown in Fig. (1). The coefficient G denotes the parametric optomagnonic coupling. We will derive it in terms of the Faraday rotation.

Relation to optomechanics.— Close to the ground state, we can treat the spin in the usual way as a harmonic oscillator, $\hat{S}_x \approx \sqrt{S/2}(\hat{b} + \hat{b}^\dagger)$, with $[\hat{b}, \hat{b}^\dagger] = 1$. Then the optomagnonic interaction $\hbar G\hat{S}_x\hat{a}^\dagger\hat{a} \approx \hbar G\sqrt{S/2}\hat{a}^\dagger\hat{a}(\hat{b} + \hat{b}^\dagger)$ becomes formally equivalent to the well-known *optomechanical* interaction [23], with bare coupling constant $g_0 = G\sqrt{S/2}$. All the phenomena of optomechanics apply, including the “optical spring” (here: light-induced changes of the magnon precession frequency) and optomagnonic cooling at a rate Γ_{opt} , and the formulas (as reviewed in Ref. [23]) can be taken over directly. All these effects depend on the light-enhanced coupling $g = g_0\alpha$, where $\alpha = \sqrt{n_{\text{phot}}}$ is the cavity light amplitude. For example, in the sideband-resolved regime ($\kappa \ll \Omega$) one would have $\Gamma_{\text{opt}} = 4g^2/\kappa$. If $g > \kappa$, one enters the strong-coupling regime, where the magnon mode and the optical mode hybridize and where coherent state transfer is possible. The connection of Eq. (1) to optomechanics was discussed previously for spin optodynamics of atomic ensembles [25], where static bistability, amplification, damping and light squeezing were studied. In contrast to such non-interacting spin ensembles, the confined magnon mode assumed here can be frequency-separated from other magnon modes.

Microscopic magneto-optical coupling G .— The Faraday effect is captured by an effective permittivity tensor that depends on the magnetization \mathbf{M} in the sample. We restrict our analysis to non-dispersive isotropic media and linear response in the magnetization, and relegate magnetic linear birefringence effects which are quadratic in \mathbf{M} (denominated the Cotton-Mouton or Voigt effect) for future work [1, 26]. In this case, the permittivity tensor acquires an antisymmetric imaginary component and can be written as $\varepsilon_{ij}(\mathbf{M}) = \varepsilon_0(\varepsilon\delta_{ij} - if\epsilon_{ijk}M_k)$, where ε_0 (ε) is the vacuum (relative) permittivity, ϵ_{ijk} the Levi-Civita tensor and f a material-dependent constant [26].

The Faraday rotation per length

$$\theta_F = \frac{\omega f M_s}{2c\sqrt{\varepsilon}}, \quad (2)$$

depends on the frequency ω , the vacuum speed of light c , and the saturation magnetization M_s . The magneto-optical coupling is derived from the time-averaged energy $\bar{U} = \frac{1}{4} \int d\mathbf{r} E_i^*(\mathbf{r}, t)\varepsilon_{ij}E_j(\mathbf{r}, t)$, using the complex representation of the field, $(\mathbf{E}^* + \mathbf{E})/2$. Note that \bar{U} is real since ε_{ij} is hermitean [1, 26]. The magneto-optical contribution is

$$\bar{U}_{MO} = -\frac{i}{4}\varepsilon_0 f \int d\mathbf{r} \mathbf{M}(\mathbf{r}) \cdot [\mathbf{E}^*(\mathbf{r}) \times \mathbf{E}(\mathbf{r})] \quad (3)$$

This couples the magnetization to the spin angular momentum density of the light field. Quantization of this expression leads to the optomagnonic coupling Hamiltonian. Its exact form will depend on the magnon and optical modes. In photonic crystals, it has been demonstrated that optical modes can be engineered by nanostructure patterning [27], and magnonic-crystals design is a matter of intense current research [28]. The electric field is easily quantized, $\hat{\mathbf{E}}^{(+)}(\mathbf{r}, t) = \sum_{\beta} \mathbf{E}_{\beta}(\mathbf{r})\hat{a}_{\beta}(t)$, where $\mathbf{E}_{\beta}(\mathbf{r})$ indicates the β^{th} eigenmode of the electric field. The magnetization requires more careful consideration, since $\mathbf{M}(\mathbf{r})$ depends on the local spin operator which, in general, cannot be written as a linear combination of bosonic modes. There are however two simple cases: (i) small deviations of the spins, for which the Holstein-Primakoff representation is linear in the bosonic magnon operators, and (ii) a homogeneous Kittel mode $\mathbf{M}(\mathbf{r}) = \mathbf{M}$ with macrospin \mathbf{S} . In the following we treat the homogeneous case, to capture nonlinear dynamics. From Eq. (3) we then obtain the coupling Hamiltonian $\hat{H}_{MO} = \hbar \sum_{j\beta\gamma} \hat{S}_j G_{\beta\gamma}^j \hat{a}_{\beta}^\dagger \hat{a}_{\gamma}$ with

$$G_{\beta\gamma}^j = -i \frac{\varepsilon_0 f M_s}{4\hbar S} \epsilon_{jmn} \int d\mathbf{r} E_{\beta m}^*(\mathbf{r}) E_{\gamma n}(\mathbf{r}), \quad (4)$$

where we replaced $M_j/M_s = \hat{S}_j/S$, with S the extensive total spin (scaling like the mode volume). One can diagonalize the hermitean matrices G^j , though generically not simultaneously. In the present work, we treat the conceptually simplest case of a strictly diagonal coupling to some optical eigenmodes ($G_{\beta\beta}^j \neq 0$ but $G_{\alpha\beta}^j = 0$). This is precluded only if the optical modes are both time-reversal invariant (\mathbf{E}_{β} real-valued) and non-degenerate. In all the other cases, a basis can be found in which this is valid. For example, a strong static Faraday effect will turn optical circular polarization modes into eigenmodes. Alternatively, degeneracy between linearly polarized modes implies we can choose a circular basis.

Consider circular polarization (R/L) in the y - z -plane, such that G^x is diagonal while $G^y = G^z = 0$. Then we find

$$G_{LL}^x = -G_{RR}^x = G = \frac{1}{S} \frac{c\theta_F}{4\sqrt{\varepsilon}} \xi, \quad (5)$$

where we used Eq. (2) to express the coupling via the Faraday rotation θ_F , and where ξ is a dimensionless overlap factor that reduces to 1 if we are dealing with plane waves (Supp. Mat. IA). Thus, we obtain the coupling Hamiltonian $H_{MO} = \hbar G \hat{S}_x (\hat{a}_L^\dagger \hat{a}_L - \hat{a}_R^\dagger \hat{a}_R)$. This reduces to Eq. (1) if the incoming laser drives only one of the two circular polarizations.

The coupling G gives the *magnon precession* frequency shift *per* photon. It decreases for larger magnon mode volume, in contrast to GS , which describes the overall *optical* shift for saturated spin ($S_x = S$). For YIG, with $\varepsilon \approx 5$ and $\theta_F \approx 200^\circ \text{cm}^{-1}$ [1, 29], we obtain $GS \approx 10^{10} \text{Hz}$ (taking $\xi = 1$), which can easily become comparable to the precession frequency Ω . The ultimate limit for the magnon mode volume is set by the optical wavelength, $\sim (1\mu\text{m})^3$, which yields $S \sim 10^{10}$. Therefore $G \approx 1 \text{Hz}$, whereas the coupling to a single magnon would be remarkably large: $g_0 = G\sqrt{S/2} \approx 0.1 \text{MHz}$. This provides a strong incentive for designing small magnetic structures, by analogy to the scaling of piezoelectrical resonators [30]. Conversely, for a macroscopic volume of $(1\text{mm})^3$, with $S \sim 10^{19}$, this reduces to $G \approx 10^{-9} \text{Hz}$ and $g_0 \approx 10 \text{Hz}$.

Spin dynamics.— We now turn to the nonlinear dynamics, where the spin differs significantly from a harmonic oscillator and deviates from optomechanics. The coupled Heisenberg equations of motion are obtained by using $[\hat{a}, \hat{a}^\dagger] = 1$, $[\hat{S}_i, \hat{S}_j] = i\epsilon_{ijk}\hat{S}_k$. We next focus on the classical limit, where we replace the operators by their expectation values:

$$\begin{aligned} \dot{a} &= -i(GS_x - \Delta)a - \frac{\kappa}{2}(a - \alpha_{\max}) \\ \dot{\mathbf{S}} &= (Ga^* \mathbf{e}_x - \Omega \mathbf{e}_z) \times \mathbf{S} + \frac{\eta_G}{S}(\dot{\mathbf{S}} \times \mathbf{S}) \end{aligned} \quad (6)$$

Here we introduced the cavity decay rate κ and the laser amplitude α_{\max} , and the intrinsic spin Gilbert-damping, characterized by η_G , due to phonons and defects ($\eta_G \approx 10^{-4}$ for YIG [31]).

After rescaling the fields (Suppl. IB), we see that the classical nonlinear dynamics is controlled by only five dimensionless parameters: $\frac{GS}{\Omega}$, $\frac{G\alpha_{\max}^2}{\Omega}$, $\frac{\Delta}{\Omega}$, $\frac{\kappa}{\Omega}$, η_G . These are independent of \hbar .

Fast cavity regime.— As a first step we study a spin slow compared to the cavity, where $G\dot{S}_x \ll \kappa^2$. In that case we can expand the field $a(t)$ in powers of \dot{S}_x . We write $a(t) = a_0(t) + a_1(t) + \dots$, where the subscript indicates the order in \dot{S}_x . From the equation for $a(t)$, we find that a_0 fulfills the instantaneous equilibrium condition

$$a_0(t) = \frac{\kappa}{2} \alpha_{\max} \frac{1}{\frac{\kappa}{2} - i(\Delta - GS_x(t))}, \quad (7)$$

from which we obtain the correction a_1 :

$$a_1(t) = -\frac{1}{\frac{\kappa}{2} - i(\Delta - GS_x)} \frac{\partial a_0}{\partial S_x} \dot{S}_x. \quad (8)$$

To derive the effective equation of motion for the spin, we replace $|a|^2 \approx |a_0|^2 + a_1^* a_0 + a_0^* a_1$ in Eq. (6) which leads to

$$\dot{\mathbf{S}} = \mathbf{B}_{\text{eff}} \times \mathbf{S} + \frac{\eta_{\text{opt}}}{S} (\dot{S}_x \mathbf{e}_x \times \mathbf{S}) + \frac{\eta_G}{S} (\dot{\mathbf{S}} \times \mathbf{S}). \quad (9)$$

Here $\mathbf{B}_{\text{eff}} = -\Omega \mathbf{e}_z + \mathbf{B}_{\text{opt}}$, where $\mathbf{B}_{\text{opt}}(S_x) = G|a_0|^2 \mathbf{e}_x$ acts as an optically induced magnetic field. The second term is reminiscent of Gilbert damping, but with spin-velocity component only along $\hat{\mathbf{x}}$. Both the induced field \mathbf{B}_{opt} and dissipation coefficient η_{opt} depend explicitly on the instantaneous value of $S_x(t)$:

$$\mathbf{B}_{\text{opt}} = \frac{G}{\left[\left(\frac{\kappa}{2}\right)^2 + (\Delta - GS_x)^2\right]} \left(\frac{\kappa}{2} \alpha_{\max}\right)^2 \mathbf{e}_x \quad (10)$$

$$\eta_{\text{opt}} = -2G\kappa S |\mathbf{B}_{\text{opt}}| \frac{(\Delta - GS_x)}{\left[\left(\frac{\kappa}{2}\right)^2 + (\Delta - GS_x)^2\right]}. \quad (11)$$

In the weak dissipation limit ($\eta_G, \eta_{\text{opt}} \ll 1$), we can evaluate further $\dot{S}_x \approx \dot{S}_{x0}$ from $\dot{\mathbf{S}}_0 = \mathbf{B}_{\text{eff}} \times \mathbf{S}_0$ and therefore obtain $\dot{S}_x \approx \Omega S_y$. This completely determines \mathbf{B}_{opt} and $\Gamma_{\text{opt}} = \eta_{\text{opt}} \Omega$ in terms of (S_x, S_y) , which allows us to evaluate the full nonlinear adiabatic dynamics of the

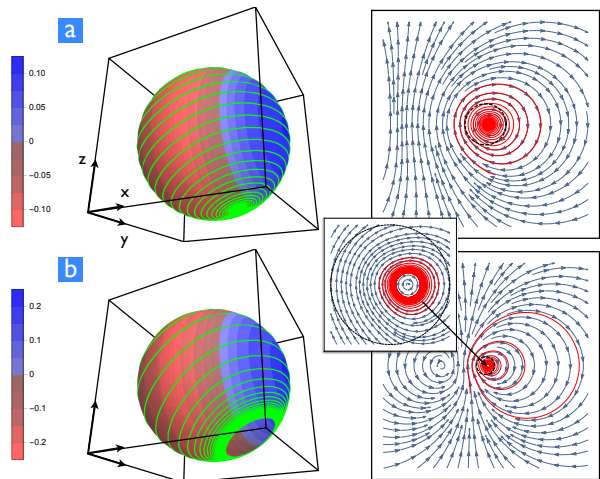


Figure 2. (Color online) Spin dynamics (fast cavity limit) at blue detuning $\Delta = \Omega$ and fixed $GS/\Omega = 2$, $\kappa/\Omega = 5$, $\eta_G = 0$. The left column depicts the trajectory (green full line) of a spin (initially pointing near the north pole) on the Bloch sphere. The color scale indicates the optical damping η_{opt} . The right column shows a stereographic projection, where the black dotted line indicates the equator (invariant under the mapping), while the north pole is mapped to infinity. The streamlines of the spin flow are also depicted. (a) Magnetization switching behavior for small light intensity $G\alpha_{\max}^2/\Omega = 0.6$. (b) Limit cycle attractor for larger light intensity $G\alpha_{\max}^2/\Omega = 0.8$.

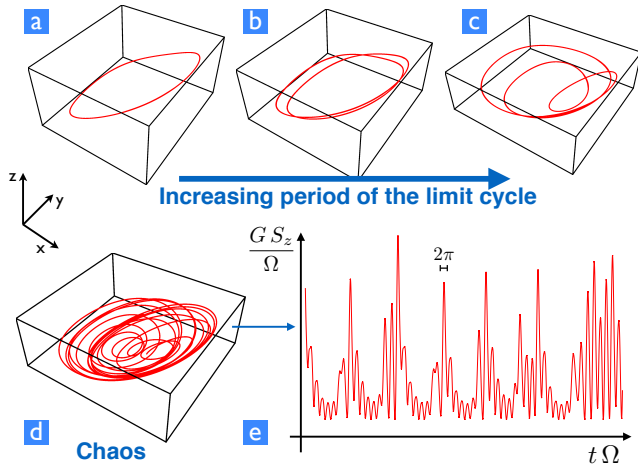


Figure 3. (Color Online) Full non-linear spin dynamics and route to chaos for $GS/\Omega = 3$ and $G\alpha_{\max}^2/\Omega = 1$ ($\eta_G = 0$). The solid red curves represent the spin trajectory after the initial transient, on the Bloch sphere for (a) $\kappa/\Omega = 3$, (b) $\kappa/\Omega = 2$, (c) $\kappa/\Omega = 0.9$, (d) $\kappa/\Omega = 0.5$. (f) S_z projection as a function of time for the chaotic case $\kappa/\Omega = 0.5$.

spin. Two distinct solutions can be found: generation of new stable fixed points (switching) and optomagnonic limit cycles, as we discuss below.

By our Hamiltonian (Eq. (1)), the north pole is stable in the absence of optomagnonic coupling – the selection of this state is ensured by the intrinsic damping $\eta_G > 0$. By driving the system this can change due to the energy pumped to (or absorbed from) the spin, and the new equilibrium is determined by \mathbf{B}_{eff} and η_{opt} , which usually dominate η_G . Magnetic switching can be obtained for blue detuning $\Delta > 0$, in which case η_{opt} is negative either on the whole Bloch sphere (when $\Delta > GS$) or on a certain region, as shown in Fig. (2)a. Similar results were obtained in the case of spin optodynamics for cold atoms systems [25]. Limit cycles can be found for $|\Delta| < GS$, where the optically induced dissipation η_{opt} can change sign on the Bloch sphere (Fig. (2)b).

Full nonlinear dynamics.– The non-linear system of Eq. (6) presents even richer behavior when we leave the fast-cavity regime. For limit cycles near the north pole, when $\delta S \ll S$, the spin is well approximated by a harmonic oscillator, and the dynamics is governed by the attractor diagram established for optomechanics [32]. This is always true slightly above the instability threshold (when the limit cycle is small), but even higher-order attractors should be observable, if their amplitudes $G\delta S \sim \Omega$ [32] remain small, requiring $GS/\Omega \gg 1$. In contrast, larger limit cycles will display novel features unique to optomagnonics, on which we focus here.

Fig. (3) shows the route to chaos by successive period doubling, upon decreasing the cavity decay κ . This route can be followed in detail as a function of any selected

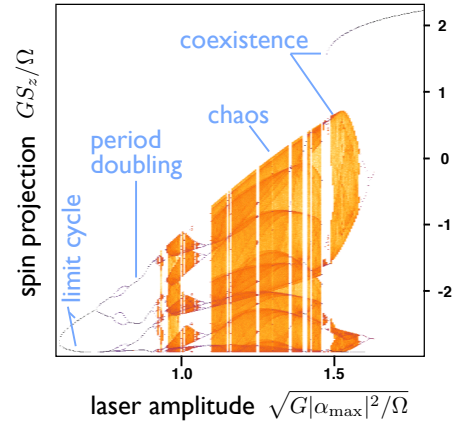


Figure 4. Bifurcation density plot for $GS/\Omega = 3$ and $\kappa/\Omega = 1$ at $\Delta = \Omega$ ($\eta_G = 0$), as a function of light intensity. We plot the S_z values attained at the turning points ($\dot{S}_z = 0$). For other possible choices (eg. $\dot{S}_x = 0$) the overall shape of the bifurcation diagram is changed, but the bifurcations and chaotic regimes remain at the same light intensities. For the plot, 30 different random initial conditions were taken.

parameter by plotting the bifurcation diagram. This is depicted in Fig. (4). The plot shows the evolution of the attractors of the system as the light intensity is increased. The figure shows the creation and expansion of a limit cycle from a fixed point, followed by successive period doubling events and finally entering into a chaotic region. At high intensities, a limit cycle can coexist with a chaotic attractor. For even bigger light intensities, the chaotic attractor disappears and the system precesses around the \hat{x} axis, as a consequence of the strong optically induced magnetic field \mathbf{B}_{opt} . Similar bifurcation diagrams are obtained by varying either GS/Ω or the detuning Δ/Ω (Supp. Mat. I C).

These nonlinear optomagnonic effects should be observable in experiments. While self-sustained oscillations and switching can be reached in the fast-cavity regime, more complex nonlinear behavior such as period doubling and chaos requires approaching sideband resolution. For YIG the examples in Figs. 3, 4 correspond to a precession frequency $\Omega \approx 3 \cdot 10^9 \text{ Hz}$ (Supp. Mat. I C), whereas κ can be estimated to be $\sim 10^{10} \text{ Hz}$, taking into account the light absorption factor for YIG ($\sim 0.3 \text{ cm}^{-1}$) [29].

Outlook.– The observation of the spin dynamics predicted here will be a sensitive probe of the basic cavity optomagnonic model, beyond the linear regime. Our analysis of the optomagnonic nonlinear Gilbert damping could be generalized to more advanced settings, leading to optomagnonic reservoir engineering (e.g. two optical modes connected by a magnon transition). In this work we focused on the homogeneous Kittel mode. It will be an interesting challenge to study the cou-

pling to magnon modes at finite wavevector, responsible for magnon-induced dissipation and nonlinearities under specific conditions [33–35]. The limit cycle oscillations (“optomagnonic lasing”) could serve as a novel source of traveling spin waves in suitable geometries, and the synchronization of such oscillators might be employed to improve their frequency stability. We may see the design of optomagnonic crystals and investigation of optomagnonic polaritons in arrays. In addition, future cavity optomagnonics experiments will allow to address the completely novel regime of cavity-assisted coherent optical manipulation of nonlinear magnetic textures, like domain walls, vortices or skyrmions, or even nonlinear spatiotemporal light-magnon patterns. In the quantum regime, prime future opportunities will be the conversion of magnons to photons or phonons, the entanglement between these subsystems, and their applications to quantum communication and sensitive measurements.

We note that different aspects of optomagnonic systems have been investigated in a related work done simultaneously [36]. Our work was supported by an ERC-StG OPTOMECH and ITN cQOM. H.T. acknowledges support by AFOSR and DARPA.

-
- [1] D. D. Stancil and A. Prabhakar, *Spin Waves* (Springer, 2009).
- [2] A. V. Chumak, V. I. Vasyuchka, A. A. Serga, and B. Hillebrands, *Nature Physics* **11**, 453 (2015).
- [3] A. A. Serga, A. V. Chumak, and B. Hillebrands, *Journal of Physics D: Applied Physics* **43**, 264002 (2010).
- [4] C. D. Stanciu, F. Hansteen, A. V. Kimel, A. Kirilyuk, A. Tsukamoto, A. Itoh, and T. Rasing, *Physical Review Letters* **99**, 047601 (2007).
- [5] A. Kirilyuk, A. V. Kimel, and T. Rasing, *Reviews of Modern Physics* **82**, 2731 (2010).
- [6] C.-H. Lambert, S. Mangin, B. S. D. C. S. Varaprasad, Y. K. Takahashi, M. Hehn, M. Cinchetti, G. Malinowski, K. Hono, Y. Fainman, M. Aeschlimann, and E. E. Fullerton, *Science* **345**, 1337 (2015).
- [7] H. Huebl, C. W. Zollitsch, J. Lotze, F. Hocke, M. Greifenstein, A. Marx, R. Gross, and S. T. B. Goennenwein, *Physical Review Letters* **111**, 127003 (2013).
- [8] X. Zhang, C.-L. Zou, L. Jiang, and H. X. Tang, *Physical Review Letters* **113**, 156401 (2014).
- [9] Y. Tabuchi, S. Ishino, T. Ishikawa, R. Yamazaki, K. Usami, and Y. Nakamura, *Physical Review Letters* **113**, 083603 (2014).
- [10] M. Goryachev, W. G. Farr, D. L. Creedon, Y. Fan, M. Kostylev, and M. E. Tobar, *Physical Review Applied* **2**, 054002 (2014).
- [11] J. Bourhill, N. Kostylev, M. Goryachev, D. Creedon, and M. Tobar, arXiv:1512.07773 (2015).
- [12] J. A. Haigh, N. J. Lambert, A. C. Doherty, and A. J. Ferguson, *Physical Review B* **91**, 104410 (2015).
- [13] L. Bai, M. Harder, Y. Chen, X. Fan, J. Xiao, and C.-M. Hu, *Physical Review Letters* **114**, 227201 (2015).
- [14] D. Zhang, X.-M. Wang, T.-F. Li, X.-Q. Luo, W. Wu, F. Nori, and J. You, *npj Quantum Information* **1**, 15014 (2015).
- [15] N. J. Lambert, J. A. Haigh, and A. J. Ferguson, *Journal of Applied Physics* **117**, 41 (2015).
- [16] Y. Tabuchi, S. Ishino, A. Noguchi, T. Ishikawa, R. Yamazaki, K. Usami, and Y. Nakamura, *Science* **349**, 405 (2015).
- [17] O. İ. O. Soykal and M. E. Flatté, *Physical Review Letters* **104**, 1 (2010).
- [18] X. Zhang, N. Zhu, C.-L. Zou, and H. X. Tang, arXiv:1510.03545 (2015).
- [19] J. A. Haigh, S. Langenfeld, N. J. Lambert, J. J. Baumberg, A. J. Ramsay, A. Nunnenkamp, and A. J. Ferguson, *Physical Review A* **92**, 1 (2015).
- [20] A. Osada, R. Hisatomi, A. Noguchi, Y. Tabuchi, R. Yamazaki, K. Usami, M. Sadgrove, R. Yalla, M. Nomura, and Y. Nakamura, arXiv:1510.01837 (2015).
- [21] X. Zhang, C.-L. Zou, L. Jiang, and H. X. Tang, arXiv:1511.03680 (2015).
- [22] C. Kittel, *Physical Review* **73**, 155 (1948).
- [23] M. Aspelmeyer, T. J. Kippenberg, and F. Marquardt, *Reviews of Modern Physics* **86**, 1391 (2014).
- [24] Note that this frequency however depends on the magnetic field *inside* the sample, and hence it depends on its geometry and the corresponding demagnetization fields.
- [25] N. Brahms and D. M. Stamper-Kurn, *Physical Review A* **82**, 1 (2010).
- [26] L. D. Landau and E. M. Lifshitz, *Electrodynamics of continuous media*, 2nd ed., edited by E. M. Lifshitz and L. P. Pitaevskii (Pergamon Press, 1984).
- [27] J. D. Joannopoulos, S. G. Johnson, J. N. Winn, and R. D. Meade, *Photonic Crystals*, 2nd ed. (Princeton University Press, 2008).
- [28] M. Krawczyk and D. Grundler, *Journal of physics: Condensed matter* **26**, 123202 (2014).
- [29] M. J. Weber, *CRC Handbook of Laser Science and Technology Supplement 2: Optical Materials* (CRC Press, 1994).
- [30] L. Fan, K. Y. Fong, M. Poot, and H. X. Tang, *Nature communications* **6**, 5850 (2015).
- [31] In the magnetic literature, η_G is denoted as α [1].
- [32] F. Marquardt, J. G. E. Harris, and S. M. Girvin, *Physical Review Letters* **96**, 1 (2006).
- [33] A. M. Clogston, H. Suhl, L. R. Walker, and P. W. Anderson, *J. Phys. Chem. Solids* **1**, 129 (1956).
- [34] H. Suhl, *Journal of Physics and Chemistry of Solids* **1**, 209 (1957).
- [35] G. Gibson and C. Jeffries, *Physical Review A* **29**, 811 (1984).
- [36] T. Liu, X. Zhang, H. X. Tang, and M. E. Flatté, Unpublished.

I. SUPPLEMENTARY MATERIAL

A. Optomagnonic coupling G for plane waves

In this section we calculate explicitly the optomagnonic coupling presented in Eq. (5) for the case of plane waves mode functions for the electric field. We choose for definiteness the magnetization axis along the \hat{z} axis, and consider the case $G_{x\beta\gamma} \neq 0$. The Hamiltonian H_{MO}

is then diagonal in the the basis of circularly polarized waves, $\mathbf{e}_{R/L} = \frac{1}{\sqrt{2}}(\mathbf{e}_y \mp i\mathbf{e}_z)$. The rationale behind choosing the coupling direction *perpendicular* to the magnetization axis, is to maximize the coupling to the magnon mode, that is to the *deviations* of the magnetization with respect to the magnetization axis. The relevant spin operator is therefore \hat{S}_x , which represents the flipping of a spin. In the case of plane waves, we quantize the electric field according to $\hat{\mathbf{E}}^{+(-)}(\mathbf{r}, t) = +(-)i \sum_j \mathbf{e}_j \sqrt{\frac{\hbar\omega_j}{2\varepsilon_0\varepsilon V}} \hat{a}_j^{(+)}(t) e^{+(-)i\mathbf{k}_j \cdot \mathbf{r}}$, where V is the volume of the cavity, \mathbf{k}_j the wave vector of mode j and we have identified the positive and negative frequency components of the field as $\mathbf{E} \rightarrow \hat{\mathbf{E}}^+$, $\mathbf{E}^* \rightarrow \hat{\mathbf{E}}^-$. The factor of $\varepsilon_0\varepsilon$ in the denominator ensures the normalization $\hbar\omega_j = \varepsilon_0\varepsilon \langle j | \int d^3\mathbf{r} |\mathbf{E}(\mathbf{r})|^2 | j \rangle - \varepsilon_0\varepsilon \langle 0 | \int d^3\mathbf{r} |\mathbf{E}(\mathbf{r})|^2 | 0 \rangle$, which corresponds to the energy of a photon in state $|j\rangle$ above the vacuum $|0\rangle$. For two degenerate (R/L) modes at frequency ω , using Eq. (2) we see that the frequency dependence cancels out and we obtain the simple form for the optomagnonic Hamiltonian $H_{MO} = \hbar G \hat{S}_x (\hat{a}_L^\dagger \hat{a}_L - \hat{a}_R^\dagger \hat{a}_R)$ with $G = \frac{1}{S} \frac{c\theta_F}{4\sqrt{\varepsilon}}$. Therefore the overlap factor $\xi = 1$ in this case.

B. Rescaled fields and linearized dynamics

To analyze Eq. (6) it is convenient to re-scale the fields such that $a = \alpha_{\max} a'$, $\mathbf{S} = S \mathbf{S}'$ and measure all times and frequencies in Ω . We obtain the rescaled equations of motion (time-derivatives are now with respect to $t' = \Omega t$)

$$\dot{a}' = -i \left(\frac{GS}{\Omega} S'_x - \frac{\Delta}{\Omega} \right) a' - \frac{\kappa}{2\Omega} (a' - 1) \quad (12)$$

$$\dot{\mathbf{S}}' = \left(\frac{G\alpha_{\max}^2}{\Omega} |a'|^2 \mathbf{e}_x - \mathbf{e}_z \right) \times \mathbf{S}' + \frac{\eta_G}{S} (\dot{\mathbf{S}}' \times \mathbf{S}') \quad (13)$$

If we linearize the spin-dynamics (around the north-pole, e.g.), we should recover the optomechanics behavior. In this section we ignore the intrinsic Gilbert damping term. We set approximately $\mathbf{S}' \approx (S'_x, S'_y, 1)^T$ and from Eq. (12) we obtain

$$\dot{S}'_x = S'_y \quad (14)$$

$$\dot{S}'_y = -\frac{G\alpha_{\max}^2}{\Omega} |a'|^2 - S'_x \quad (15)$$

We can now choose to rescale further, via $S'_x =$

$(\alpha_{\max}/\sqrt{S}) S''_x$ and likewise for S'_y . We obtain the following spin-linearized equations of motion:

$$\dot{S}''_x = S''_y \quad (16)$$

$$\dot{S}''_y = -\frac{G\sqrt{S}\alpha_{\max}}{\Omega} |a'|^2 S''_x \quad (17)$$

$$\dot{a}' = -i \left(\frac{G\sqrt{S}\alpha_{\max}}{\Omega} S''_x - \frac{\Delta}{\Omega} \right) a' - \frac{\kappa}{2\Omega} (a' - 1) \quad (18)$$

This means that the number of dimensionless parameters has been reduced by one, since the two parameters initially involving G , S , and α_{\max} have all been combined into

$$\frac{G\sqrt{S}\alpha_{\max}}{\Omega} \quad (19)$$

In other words, for $S'_{x,y} = S_{x,y}/S \ll 1$, the dynamics should only depend on this combination, consistent with the optomechanical analogy valid in this regime as discussed in the main text (where we argued based on the Hamiltonian).

C. Nonlinear dynamics

In this section we give more details on the full nonlinear dynamics described in the main text. In Figs. 3 and (4) of the main text we chose a relative coupling $GS/\Omega = 3$, around which a chaotic attractor is found. With our estimated $GS \approx 10^{10}$ Hz for YIG, this implies a precession frequency $\Omega \approx 3 \cdot 10^9$ Hz. In Fig. (3) the chaotic regime is reached at $\kappa \approx \Omega/2$ with $G\alpha_{\max}^2/\Omega = 1$, which implies $\alpha_{\max}^2 \approx S/3$, that is, a number of photons circulating in the (unperturbed) cavity of the order of the number of locked spins and hence scaling with the cavity volume. Bigger values of the cavity decay rate are allowed for attaining chaos at the same frequency, at the expense of more photons in the cavity, as can be deduced from Fig. (4) where we took $\kappa = \Omega$. On the other hand we can think of varying the precession frequency Ω by an applied external magnetic field and explore the nonlinearities by tuning GS/Ω in this way (note that GS is a material constant). This is done in Fig. (5). Alternatively, the nonlinear behavior can be controlled by varying the detuning Δ , as shown in Fig. (6).

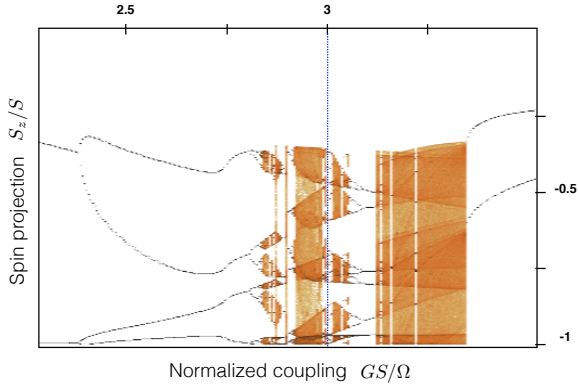


Figure 5. (Color online) Bifurcation density plot for $G\alpha_{\max}^2/\Omega = 1$ and $\kappa/\Omega = 1$ at $\Delta = \Omega$ ($\eta_G = 0$), as a function of the relative coupling strength GS/Ω . The dotted blue line indicates $GS/\Omega = 3$, for comparison with Fig. (4). As in the main text, the points (obtained after the transient) are given by plotting the values of S_z attained whenever the trajectory fulfills the turning point condition $\dot{S}_z = 0$, for 20 different random initial conditions.

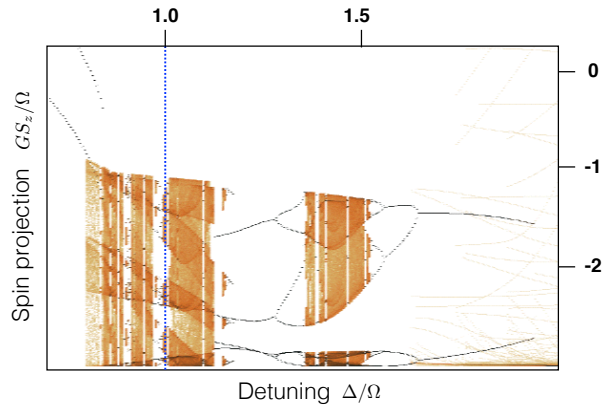


Figure 6. (Color online) Bifurcation density plot for $GS/\Omega = 3$, $G\alpha_{\max}^2/\Omega = 1$ and $\kappa/\Omega = 1$ ($\eta_G = 0$), as a function of the detuning Δ/Ω . The dotted blue line indicates $\Delta/\Omega = 1$, for comparison with Fig. (4).